J Mater Sci (2007) 42:4778–4784
DOI 10.1007/s10853-006-0741-0

Synthesis and physical properties of new oxide $AgMnO_2$

Nesrine Koriche · Aissa Bouguelia · Mohamed Mohammedi · Mohamed Trari

Received: 6 October 2005 / Accepted: 31 July 2006 / Published online: 19 March 2007

Abstract A novel oxide $AgMnO_2$ was prepared from $LiMnO_2$ via $Ag^+ \rightarrow Li^+$ exchange in the eutectic melt $AgNO_3$-KNO_3. It crystallizes in a monoclinically distorted unit cell (SG *C2/m*) caused by the Jahn-Teller (*J-T*) ion Mn^{3+} ($3d^4$). The structure was refined by isotypy with the crednerite $CuMnO_2$. There are two long axial Mn–O of 264.2(0) pm and four equatorial bonds of 192.7(3) pm and Mn–O–Mn adjoining (83.07°) are bent below the ideal angle. The thermal variation of the magnetic susceptibility (χ/T^{-1}) obeys a Curie-Weiss law with manganese in a trivalent, high spin (HS) state accommodated in elongated MnO_6 octahedra (14.8%). Direct coupling between Mn^{3+} involves negative exchange interactions through long-range antiparallel moments with a temperature θ_p = –436 K and a magnetic moment of 5.26 μ_B/Mn^{3+} slightly larger than the spin only moment. The title oxide is stable in air up to ~680 °C before it decomposes into metal silver. It displays a semi-conducting behavior with an activation energy of ~0.45 eV, characteristic of a conduction by low mobility polarons between $Ag^{+/2+}$ where nearly all polarons are bonded. The photoelectrochemical properties of $AgMnO_2$ have been investigated by photocurrent technique in 1 M KOH. The cathodic photocurrent J_{ph} provides unambiguous evidence of *p*-type character attributed to oxygen insertion (0.025 oxygen by formula unit) as required by the charge compensating mechanism. The valence band is made up of Ag–4*d* wave functions positioned at ~5.14 eV below vacuum. A comparison with $CuMnO_2$ was also reported.

N. Koriche · A. Bouguelia · M. Trari (✉)
Faculté de Chimie, Laboratoire de Stockage et de Valorisation des Energies Renouvelables, USTHB, BP 32, 16111 Algiers, Algeria
e-mail: mtrari@caramail.com

M. Mohammedi
Ecole Polytechnique EMP, BP 17, Algiers, Algeria

Introduction

Until quite recently there was an increasing interest on delafossites $A^+M^{3+}O_2$, where A denotes Cu or Ag and M any one of *3d* cations, owing to their applications in the solar energy conversion [1] and utilization as transparent thin film [2]. We have already introduced the idea that hydrogen may insert between $\{MO_2^-\}_\infty$ sheets to form intercalation compounds, one of the central topic in the high energy cells; the basic structure is not altered [3] and suggest that they are potential solar energy convectors [4].

Unlike to copper, only few papers have been devoted to Ag delafossites which concern the synthesis and structural characterization [5]. The reason is that the Ag related compounds generally possess a poor thermal stability which makes difficult their preparation from direct reaction. Doubt about the existence of $AgMnO_2$ was raised early [6] where the authors were unable to prepare it by solid state reaction because of the small free energy of formation $\Delta G°_f$ of Ag_2O (–11.2 kcal mol^{-1}) resulting in a low temperature decomposition (~230 °C) [7]. As far as the authors are aware, there does not exist any paper in the literature concerning this oxide and no attempts appear to have been made to extend the studies to ternary phase diagram Ag–Mn–O. Mn^{3+}, possessing four unpaired

spins, is subjected to a strong *J-T* distortion, observed in the asymmetry of MnO_6 octahedra. The ideal delafossite has a simple hexagonal symmetry but the tilting of MnO_6 octahedra around the [100] direction leads to a larger unit cell and a lower symmetry. The monoclinic structure, unique among $Ag^{I}M^{III}O_2$ congeners, is corroborated by an unusually large *c/a* value. In octahedral coordination field, HS Mn^{3+} would have the electronic configuration (^5D, t_{2g}^3 e_g^1) and support our finding of two longer apical and four shorter equatorial Mn–O distances. This paper deals with the synthesis, the physical and photoelectrochemical properties of $AgMnO_2$ prepared by exchange reaction between $LiMnO_2$ and $AgNO_3$. Interestingly, the precursor $LiMnO_2$ is not isotypic, it adopts an orthorhombic variation of NaCl structure, ascribed to *J-T* effect of Mn^{3+} with an ordering of Mn^{3+} and Li^+ along the *c*-axis. The refinement of $AgMnO_2$ was made by isotypy with the crednerite $CuMnO_2$ whose structure has been determined on single crystals [8].

Experimental

$AgMnO_2$ was prepared by modifying slightly our previous method (manuscript in preparation). In the present case, the reaction takes place in an oxidizing flux consisting on the eutectic melt $AgNO_3$-KNO_3 (39 mol.% KNO_3, $T_{eut.}$ ~130 °C):

$$LiMnO_2 + AgNO_3 \rightarrow AgMnO_2 + LiNO_3$$

the mixture was heated in a closed Pyrex ampoule for one week at 250 °C and the product was recovered as black powder by leaching with demineralized water. A slight excess of $AgNO_3$ (ratio 1.1) must be used to preclude formation of silver metal, detected by optical microscopy and X-ray diffraction (XRD). On the contrary, with silver deficiency, $AgMn_2O_4$ was favored as can be seen from additional peaks in the XRD pattern. $LiMnO_2$ was prepared from Li_2CO_3 (with a 5% weight excess) and Mn_2O_3. The homogenous mixture was fired under pure argon flow at 800 °C with an isothermal step of 6 h at 500 °C to preclude loss of lithium followed by formation of spinel $LiMn_2O_4$. Argon was deoxygenated by passing the gas over a bed of iron filling at 500 °C. Excellent Mn_2O_3 was obtained by heating pure MnO_2 at 850 °C overnight and air quenched. For comparison purpose, isotypic $CuMnO_2$ was prepared very pure from stoichiometric amounts of CuO and MnO both of purity >99.9% in evacuated silica ampoule and heated at 980 °C. Two regrindings are required to get well-crystallized oxides. The phases were identified by XRD using a monochromatized Cu-$K\alpha$ radiation, the diffraction data were collected by 0.2° step over a 2θ range from 5° to 80°. The lattice constants were refined by the least square method from corrected *d*-values using Si as standard. The density was measured by the hydrostatic method using toluene because of its excellent wetting property. The thermal stability range was determined by coupled TG/DTG analysis in a Setaram thermobalance (Setsys 16/18) and the oxygen content was established with an accuracy of ±0.01. The infrared spectra was obtained by employing the KBr disk technique in a Brucker type Vector 22 spectrometer (resolution < 2 cm^{-1}) instrument. The Mn oxidation state, evaluated from iodometry, was found to be 1 ± 0.01 in agreement with the chemical formula and the ratio Ag/Mn ratio was obtained from inductively coupled plasma (ICP) spectroscopy (Vista-PRO-CCD). The magnetic susceptibility χ(T), corrected from diamagnetism of relevant ions [7], was measured in a magnetic balance under a field of 20,000 G from 740 °C down to liquid helium. Sixty-five percent dense pellets were prepared by sintering pellets at 450 °C and the conductivity σ was measured by the collinear four probe method. Electrical contact on the back surface was made with silver cement to which a copper wire was soldered, the electrode was then encapsulated in a glass holder with epoxy resin. Electrochemical measurements were done in a 1 M KOH electrolyte deaerated by nitrogen bubbling. The working electrode was potentiostated against a saturated calomel electrode (SCE) using a Voltalab PGP201 potentionstat. A platinum electrode, treated in concentrated HNO_3, was employed as auxiliary electrode. In order to determine with exactitude the flat band potential V_{fb}, hand-chopped light from a 200 W tungsten lamp was used with a light flux at the electrode surface of 74 mW cm^{-2}. The solutions were prepared from analytical reagents and twice distilled water.

Results and discussion

Ion exchange reactions in molten salts are shown to be a general feature that offer an unexplored route for the preparation of new phases of inorganic oxides not accessible by solid reactions. Although the precursor $LiMnO_2$ crystallizes in an ordered NaCl structure, the exchange takes places easily with a small motional enthalpy as is evidenced from the low synthesis temperature. This illustrates that the exchange occurs even in the absence of cations vacancies and thermodynamically, it is favored with ions of comparable

mobilities namely Li^+ and Ag^+. No trace of $AgMn_2O_4$ was detected and the Ag/Mn ratio, obtained by ICP, was found to be very close to unity within the experimental errors (Ag/Mn ~ 1.01). The structural refinement was made with the space group *C2/m* (N°12) and the positional parameters of $CuMnO_2$. The hybridized sp^3 oxygen is tetrahedrally coordinated by three manganese and one silver and its position involves only one variable parameter. The monoclinic distortion results from a strong *J-T*-like elongation of MnO_6 octahedra. The precise parameters are listed in Table 1 together with the observed and calculated *d*-interplanar spacings. The experimental density (6.371 g cm^{-3}) is close to that calculated on the base of two formula weights by unit cell (6.470 g cm^{-3}).

The anisotropic structure contains a closed packed layers of infinite sheets of edge shared octahedra $\{MnO_2^-\}_\infty$ interleaved with layers containing exclusively Ag^+ (Fig. 1). Each silver is hexagonally coordinated by six other silvers in the basal plane and linearly bonded to two oxygen forming $(AgO_2)^{3-}$ ''dumb-bell'' parallel to *c*-axis.

Ag(I) shows a pronounced tendency towards twofold coordination because of the relatively small energy difference between filled value *5s*-orbital and *4d*-orbital [9] which permits a good overlap unlike to cadmium that does not enjoy linear sites. Indeed, the electric charge corresponding to the hybrid orbital $(d_{z2}+s)/\sqrt{2}$ is located in a plane perpendicular to

Table 1 Powder X-ray data of $AgMnO_2$ obtained by isotypy with $CuMnO_2$ a = 558.3(9) pm, b = 289.4(6) pm, c = 629.3(5) pm, β = 100.6(2), Space Group *C2/m*

h k l	$d_{obs.}$	$d_{calc.}$	Intensity
0 0 1	6.1989	6.17449	20
0 0 2	3.0924	3.08725	100
2 0 0	2.7408	2.74413	59.8
1 1 0	2.5585	2.56032	29.1
1 1 –1	2.4399	2.44100	73.4
1 1 1	2.2952	2.29693	35.4
0 0 3	2.0601	2.06120	9.8
2 0 2	1.8879	1.8873	10
	1.7601[a]		0.8
1 1 –3	1.6782	1.67791	12.4
	1.5912		0.9
3 1 –1	1.5563	1.55849	15.4
1 1 3	1.5447	1.54242	15.1
	1.4737[a]		2
2 0 –4	1.4681	1.46789	2.5
3 1 1	1.4475	1.44813	11.4
0 2 1	1.4121	1.40924	1
3 1 –3	1.3401	1.34153	3.2
0 2 2	1.3114	1.31087	4.8
2 2 0	1.2802	1.28016	6.1
2 2 –2	1.2214	1.22050	2.9

[a] Nonindexed peaks

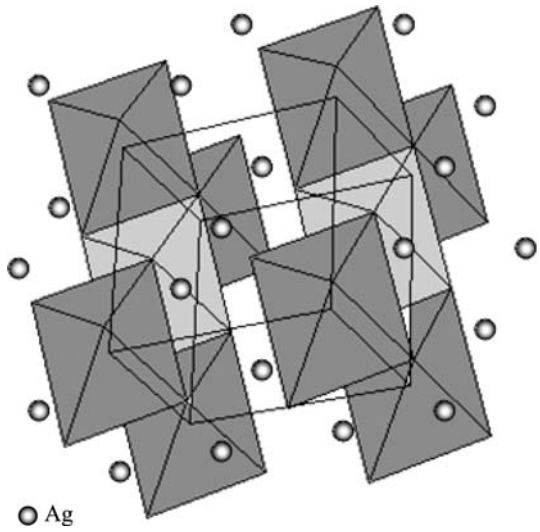

Fig. 1 The layered crystal structure of $AgMnO_2$, showing MnO_6 octahedra and O–Ag–O sticks

c-axis and lowers the electrostatic energy [10]. The accurate Ag–O length (209.1 pm) is only slightly larger (~2%) than that calculated (205.0 pm) from effective ionic radii Ag^+(II) and O^{2-}(IV) tabulated in ref. [11] confirming the linearity of Ag^+ ions and the ionicity of the chemical bond Ag–O. On the contrary, the interionic lengths Mn–O disagree with that calculated from the sum of ionic radii. The MnO_6 octahedra is strongly elongated and lowers the symmetry to monoclinic $\left(d''_{MnO}/d^{\perp}_{CuO}=1.17\right)$. The significant elongation (14.8%) is brought about by Mn^{3+} in which there are four in plane Mn–O bonds at 192.7(3) pm and two apical Mn–O bonds at 226.4(2) pm. Selected interatomic distances and bond angles are given in Table 2. The MnO_6 octhedra leads to a zigzag shaped rows along the [100] direction doubling thus the *b*-parameter with the Mn–O–Mn bonds adjoining octahedra (83.07°) bent below the ideal bond angle of 90°. We

Table 2 Selected interatomic lengths (pm) of $AgMnO_2$

Mn–O^{i}	(x4)	192.73
Mn–O^{i}	(x2)	226.42
Ag–O^{iii}	(x2)	209.12
Ag–Ag^{iv}	(x4)	304.55
Ag–Ag^{v}	(x2)	289.79
Bond angle (°) of $AgMnO_2$		
Ag–O–Ag	(x4)	94.50(1)
O–Ag–O	(x1)	180
O–Mn–O	(x4)	96.93(1)
O–Mn–O	(x2)	180
Ag–O–Mn	(x2)	96.93(1)
Ag–O–Mn	(x2)	119.24(1)
O–Mn–O	(x4)	96.93(1)
O–Mn–O	(x4)	83.07(1)

have tried to reproduce this ion exchange with another crednerite and our attempts to prepare $PdMnO_2$ in silica tube ($LiMnO_2$ + Pd + $PdCl_2$, 500 °C) have so far been unsuccessful yielding PdO probably because of its low free energy.

In order to study the stability of $AgMnO_2$ and to determine the oxygen content, we have carried out a combined TG/DTG analysis in air (Fig. 2). To our surprise and unlike to most Ag-related oxides, $AgMnO_2$ is thermally stable up to ~680 °C before to be reduced irreversibly, the dark residue in the TG experiment was a mixture of Ag and Mn_2O_3, as checked by XRD. A weight loss of 4.49% was observed between 200 and 800 °C, in agreement with that calculated (4.11%). The well-known stoichiometry of Mn_2O_3 allows an accurate determination of oxygen content (2.025). In order to know whether Mn_2O_3 is stoichiometric or not at 900 °C (the final temperature in TG plot) we have heated MnO_2 (purity > 99%) overnight at 900 °C. This temperature belongs to the stability range of Mn_2O_3 in the phase diagram. About 158 mg of Mn_2O_3 were dissolved with an execs of Mohr Salt in concentric acid. The remaining Fe^{2+} was accurately back titrated by $KMnO_4$. The oxidation state was exactly equal to 3.00. The DTG plot exhibits an anomaly at ~720 °C indicating a two steps reduction process, indeed there are two varieties of black Mn_2O_3, referred to as α- and γ-forms related in the same way as Fe_2O_3, which converts reversibly to each other at around this temperature.

The infrared spectra, given in Fig. 3, is essentially featureless between 4,000 and 1,000 cm^{-1} and no peak ascribed to –OH group (3,500 cm^{-1}) could be detected indicating that $AgMnO_2$ is not hygroscopic. The distinctive band centered at 556 cm^{-1} corresponds to stretching frequency of AgO_2^{3-} in which Ag^+ is linearly coordinated. For $CuMnO_2$, an isotopic shift toward lower energy of peak CuO_2^{3-} (650 cm^{-1}) [3] indicates a shorter Cu–O length (183.4 pm) and consequently a less ionic bond, a feature corroborated by a smaller gap E_g ($\approx 2\ E_a$) of 0.90 eV (Table 3) and a lower conductivity σ ($1.6 \times 10^{-6}\ \Omega^{-1}\ cm^{-1}$) for $AgMnO_2$ (see below). On the other hand, the large isotypic shift of $LiMnO_2$ (200–300 cm^{-1}) [12] confirms the ionicity of Li–O bond, a result consistent with the easy $Ag^+ \rightarrow Li^+$ exchange.

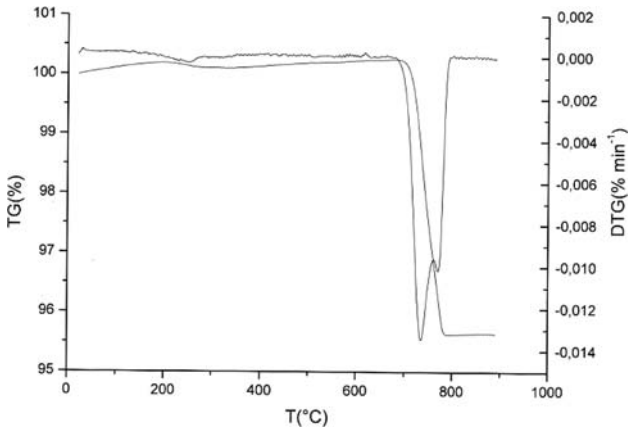

Fig. 2 Combined TG/DTG plots of $AgMnO_2$ in air

The thermal variation of the magnetic susceptibility χ^{-1}(T) is reported in Fig. 4. The large minima $d\chi^{-1}/dT$ observed at ~140 K is characteristic of a low dimensionality with a transition from para- to antiferromagnetism, typical of antiferromagnet whose intraplane interactions are of same order of magnitude than the thermal energy kT. The localization of d_{z2} electrons is partially due to the 2D character of the structure. At high temperature, χ(T) follows a Curie Weiss law i.e. $\chi = C/(T-\theta)$. The curve, fitted in the paramagnetic region indicates a strong antiferromagnetic ordering of Mn^{3+} bearing spins $S(=2)$ with $\theta_p = -436$ K and a magnetic moment of 5.26 μ_B ($C = 3.46$) slightly larger than the spin only moment for HS Mn^{3+} ($2\sqrt{S(S+1)}$, $\mu_{eff} = 4.89\ \mu_B$); however such values have been observed in some manganates [13]. Unlike $CuMnO_2$, χ(T) is not hampered by small spontaneous moment due to spin canting. In ionic oxides, the electronic configuration is nearly unaffected and exchange interactions would be anticipated with an energy $W_{ex} = -2\ J\ S_i.S_j$. As Mn-magnetic layers are separated by three nonmagnetic sheets, a good realization of 2D-antiferromagnet model would be dominated with interaction expected between half filled d^1_{z2} of Mn^{3+} through edge shared octahedra resulting from antiparallel coupling of spins S_i and S_j. The 2D-model is appropriate to estimate the integral J within $(MnO_2)^{n-1}_n$ layers. We have used an expansion of χ^{-1} in increasing powers of T^{-1}, the coefficients have been determined for an antiferromagnetic model $\left(H = 2\sum \vec{S}_i\vec{S}_j\right)$ up to 6th power for different lattices including the triangular one [14]:

$$\frac{Ng^2\mu^2}{|J|x_M}B = \frac{3}{S(S+1)}\sum\nolimits_{n=0}^{\infty} b_n(|J|/kT)^{n-1}$$

The curve corresponds to series expansion limited to 6th power. The fitted curve with $S = 2$, $g = 2$ and $J/k = -13.4$ K shows a good adjustment for $350 < T < 900$ K, below 350 K the 6th term cannot be neglected. The J/k values are correlated to Mn–Mn distance (= a parameter), the large Mn–Mn distance weakens magnetic interactions and as expected, J decreases from Ag- to $CuMnO_2$ (Table 3).

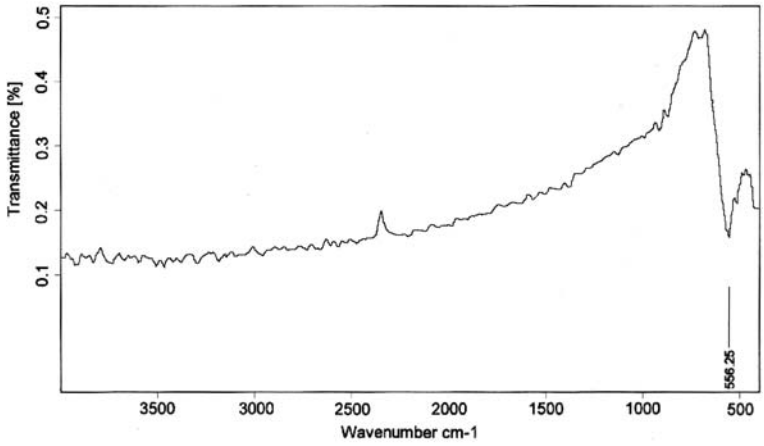

Fig. 3 The infrared spectra of $AgMnO_2$

Mixed valence oxides represent an example of intramolecular electron transfer which contain ions of same element with different oxidation states located in equivalent crystallographic sites. They belong to the class I in the Day and Robin classification with a small difference in their energies [15]. The ground state of Mn^{3+} ion is ^5D and in octahedral crystal field of O_h symmetry splits in a low ^5E_g state and an excited $^5T_{2g}$ state. Because of the *J-T* ion Mn^{3+}; the e_g orbital splits into a highest d_{x2-y2} and a lowest d_{z2} bands, the latter becomes the most stable of the two. One of us has found the same surrounding for Mn^{3+} in isostructural $CuMnO_2$ and corroborates the configuration t_{2g}^3 $d^0{}_{z2}$–$d^1{}_{x2-y2}$ with however a low distorted unit cell [8].

The Ag–Ag distance (289.4 pm) is slightly longer than that of metallic silver (288.9 pm) [7] and $AgMnO_2$ is predicted to be a semiconductor according to the band schema proposed in ref. [16]. The electrical conductivity σ of $AgMnO_2$ (Fig. 5) shows clearly a semiconducting behavior ($d\sigma/dT > 0$). The variation of log σ vs. T^{-1} follows an Arrhenius-type law ($\sigma = \sigma_0 e^{-E_a/kT}$) with an activation energy E_a (= 0.45 eV) thermally activated. E_a being the sum of the energy required to generate carriers and the activation associated with the intrinsic hopping of small polarons. The anomaly observed at ~620 °C correspond to the irreversible decomposition into metal silver (see thermal analysis). The occurrence of *p*-type conductivity is attributed to incorporation of a small amount of oxygen (0.025 oxygen/unit formula) via a balance charge to generate positive holes which involves the redox process $Ag^+ \rightarrow Ag^{2+}$ in the layered lattice. The positive thermopower $S_{300\,K}$ (+ 1,170 μV/K) indicate that the majority carriers are holes and for small polarons hopping *S* is given by [17]

$$S = -k/e\ \{\Delta E/kT + A\} = (k/e)\ln\ (N_o/N_A) = E_a$$

The constant *A* involving the entropy of transport can be neglected for small polarons. N_o/N_A is the ratio of free carriers and available sites, assimilated to the concentration of Ag^+ and calculated from the experimental density (1.97×10^{22} cm^{-3}). N_o/N_A (1.28×10^{-6}) is smaller than that predicted on the basis that each inserted oxygen yields two holes (~10^{-3}) leading to trapping of surface holes in surface-polaron states. The maximal value of N_A determined from the oxygen excess is equal to 2.5×10^{16} cm^{-3}.

Considering the potential of this new oxide, it was of interest to study its photoelectrochemical properties and to determine the electrochemical stability range. Silver could be oxidized electrochemically in two steps, the intensity-potential *J*(V) curves of $AgMnO_2$ in 1 M KOH shows an oxidation plateau between 0.30 and 0.95 V just before the oxygen evolution (Fig. 6, inset). These potentials correspond in the *E*–pH diagram of silver to equilibrium of Ag(II) oxyhydroxides. The

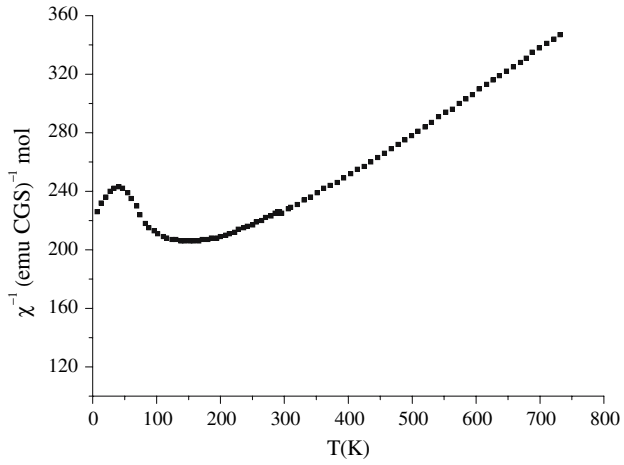

Fig. 4 The thermal variation of the reciprocal magnetic susceptibility χ^{-1} of $AgMnO_2$

Table 3 Comparative table giving some physical parameters of $AMnO_2$

$AMnO_2$	Mn–Mn (pm)	T_N (K)	J/k (K)	E_g (eV)	$\sigma_{300\ K}(\Omega\ cm)^{-1}$	$S_{300\ K}$ ($\mu V/K$)	V_{fb} (V_{SCE})
$CuMnO_2$	288.50	64[a]	–14.0	1.0	2×10^{-5}	550	+0.15
$AgMnO_2$	289.46	38	–13.4	0.9	1.6×10^{-6}	1170	–0.06

[a] Determined from Mossbauer spectroscopy according to ref. [8]

hysterisis between forward and reverse directions is typical of electrochemical transformations of the surface. The peak O (~0.6 V) can be attributed to the electrooxidation of Ag^+ and the process may be written as follows:

$$AgMnO_2 + 2\varepsilon OH^- \rightarrow AgMnO_{2+\varepsilon} + \varepsilon H_2O + 2\varepsilon e^-$$

ε stands for the amount of inserted oxygen and can be estimated from the anodic wave. The charge, independent of voltage scan rate, averaged 12 mC. Admitting that the surface is proportional to the number of oxidized sites this charge more or less corresponds to ~$10^{15}Ag^{2+}/cm^2$. Above ~1.5 V, the current shoots up considerably due to H_2O discharge. Upon the reverse potential scan, the cathodic peak *R* at ~–0.64 V is ascribed to $Ag^{2+/+}$ and the reduction corresponds to the desintercalation of oxygen excess. This situation looks similar to that observed over Ag/AgO [18] with somewhat different potentials, the discrepancy is due to the oxydo-reduction of Ag^+ on different substrates. The significant amount of current passed below –1.5 V is ascribed to H_2 evolution (H_2 bubbles were noticeable on the electrode). If the applied potential is slowly sweep down while the oxide is illuminated there will be a potential at which the photocurrent J_{ph} just appears. In order to accurately determine the transient photocurrent V_{on}, intermittent illumination was used, the light was chopped mechanically where both the irradiation and interruption were 5 s. J_{ph} was observed when the potential was cathodic of V_{on} (–0.06 V). This potential, assimilated to V_{fb} gives the position of valence band (VB) in the electrochemical scale with respect to SCE whose zero is located at 4.75 eV below vacuum. The position *P* of VB edge is given by:

$$P = eV_{fb} + \Delta E + 4.75$$

The calculated value (5.14 ± 0.1 eV) does not agree with a VB made up of Ag-*4d* wave functions. J_{ph} rose slowly without reaching a saturation, a behavior attributed to a zero electron–hole recombination. As expected, $AgMnO_2$ electrode exhibited a pH-independent potential in the range pH (7–13.5). The highest full band (VB), derived from AgO_2^{3-} units is ~1 eV positive of O^{2-}-2*p* level whereas the lowest empty level is the antibonding σ^* conduction band made up of hybrid wave functions of $5s/4d_{z2}$ orbitals, some 2 eV above the O^{2-}-2*p* level and must be less deeper than the homologous $4s/3d_{z2}$ orbitals in Cu-delafossites. The electropositive character of silver leads to a weaker covalency of Ag–O bond and consequently to a smaller destabilization of antibonding σ^*. VB is made up of nonbonding t_{2g} orbital which remains nearly constant regardless of the nature of M^{3+} ion. This results in a lager electron affinity and a smaller gap E_g and can be

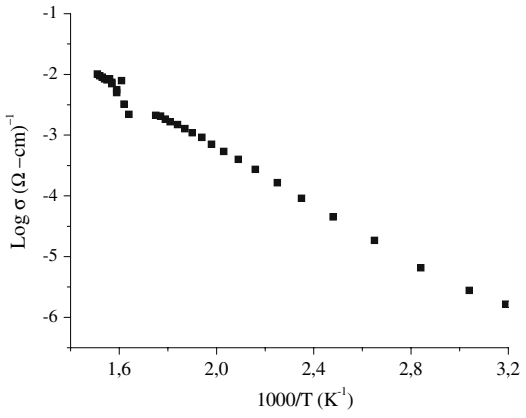

Fig. 5 Thermal dependence of the electrical conductivity σ of $AgMnO_2$

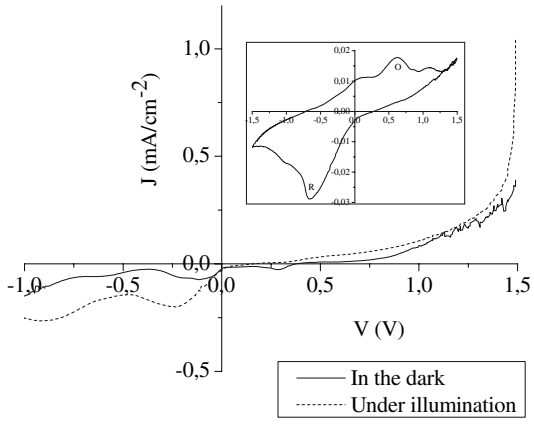

Fig. 6 The *J*(V) characteristics of $AgMnO_2$ electrode in 1 M KOH solution. Scanning rate 5 mV/s. Inset: Cyclic voltammetry in the dark

inferred from the relative atomic energy levels of Cu and Ag, with the Ag 5*s* being 0.54 eV higher than the Cu 4*s* [9].

Conclusion

The exchange reaction is a useful technique for the preparation of Ag-based oxides which proceeds with a relatively low activation energy. The present work describes the successful synthesis of new oxide Ag-MnO_2 by exchange reaction accomplished at low temperatures. Direct synthesis from oxides was not possible, yielding metallic silver. The oxide has a high thermal stability and has been characterized chemically and structurally. The crystal structure was elucidated from powder X-ray diffraction by isotypy with CuMnO$_2$. It crystallizes in a monoclinic structure, the irregular octahedra are elongated along the *c*-axis, consistent with the *J-T* ion Mn^{3+}. Octahedral-site Mn(III) would have the localized-electron configuration, the magnetic susceptibility exhibits a sharp minimum characteristic of low dimensionality; it reveals strong antiferromagnetic interactions between half filled d_{z2} through edge shared octahedra and a magnetic moment close to the spin only moment of HS Mn^{3+}. The thermal evolution of the electric resistivity is characteristic of a semiconducting behavior with an activation energy in conformity with a mechanism conduction by small polarons hopping. The *p*-type behavior is ascribed to a small oxygen overstoichiometry in the layered lattice resulting in a mixed silver valency. The electropositivity of silver promotes a certain covalency of Mn–O bond which tends to increase the Ag–O length and weakens the chemical bond. The splitting between t_{2g} VB and σ^* CB arising from a mixing $4d_{z2}/5s$ orbitals results in a destabilization of CB with a smallest electron affinity and a larger E_g value. The valence band, made up of Ag-4*d* orbitals, does not agree with that revealed from photoelectrochemical measurements.

Acknowledgements This work was supported financially be the Faculty of Chemistry (Algiers) under the contract N° E1602/04/2000. The authors are grateful to Mr A. Mokhtari for his general assistance.

References

1. Younsi M, Bouguelia A, Aider A, Trari M (2005) J Solar Energy 78:574
2. Mugnier E, Barnabe A, Tailhades P (2006) Solid State Ionics 177:607
3. Koriche N, Bouguelia A, Aider A, Trari M (2005) Int J Hydrogen Energy 30(7):693
4. Koyanagi T, Harima H, Yanase A, Katayama-Yoshida H (2003) J Phys Chem Solids 64:443
5. Clayton JE, Cann DP, Ashmore N (2002) Thin Solid Films 411:140
6. Rienacker VG, Werner K (1963) Z Anorg Allg Chem 320:141
7. Handbook of chemistry and physics, 78th edn. 1997–1998. Editor-in-Chief David R. Lide, CRC Press
8. Toper J, Trari M, Gravereau P, Chaminade JP, Doumerc JP (1995) Z Krist 210:184
9. Fraga S, Karwowski J, Saxena KMS (1976) Handbook of atomic data. Elsevier Scientific Publishing Company, Amsterdam
10. Rogers DB, Shannon RD, Prewitt CT, Gillson JL (1971) Inorg Chem 10:723
11. Shannon RD (1976) Acta Cryst A32:751
12. Hewston TA, Chamberland BL (1987) J Phys Chem Solids 48:97
13. Tabushi M, Ado K, Koyashi H, Kageyama H, Masquelier C, Kondo A, Kano R (1998) J Electrochem Soc 145(4):L46
14. Rushbrooke GS, Wood PJ (1963) Mol Phys 6:409
15. Day P, Robine R (1966) Adv Inorg Chem 10:247
16. Buljan A, Alemany P, Ruiz E (1999) J Phys Chem B 103:8060
17. Trestmann-Matts A, Dorris SE, Kumarakrishnan S, Mason TO (1983) J Am Ceram Soc 66(8):589
18. Jiang Z, Huang S, Qian B (1994) Electrochim Acta 39:2465